

# UC San Diego

## UC San Diego Previously Published Works

### Title

WNT Stimulation Dissociates a Frizzled 4 Inactive-State Complex with G $\alpha$ 12/13.

### Permalink

<https://escholarship.org/uc/item/3hd7v6j9>

### Journal

Molecular Pharmacology, 90(4)

### Authors

Arthofer, Elisa

Hot, Belma

Petersen, Julian

et al.

### Publication Date

2016-10-01

### DOI

10.1124/mol.116.104919

Peer reviewed

# WNT Stimulation Dissociates a Frizzled 4 Inactive-State Complex with $G\alpha_{12/13}$

Elisa Arthofer,<sup>1</sup> Belma Hot,<sup>1</sup> Julian Petersen, Katerina Strakova, Stefan Jäger, Manuel Grundmann, Evi Kostenis, J. Silvio Gutkind, and Gunnar Schulte

Section of Receptor Biology and Signaling, Department of Physiology and Pharmacology, Karolinska Institutet, Stockholm, Sweden (E.A., B.H., J.P., K.S., S.J., G.S.); Section on Molecular Signal Transduction, Eunice Kennedy Shriver National Institute of Child Health and Human Development, National Institutes of Health, Bethesda, Maryland (E.A.); Faculty of Science, Institute of Experimental Biology, Masaryk University, Brno, Czech Republic (K.S., G.S.); Molecular, Cellular and Pharmacobiology Section, Institute for Pharmaceutical Biology, University of Bonn, Bonn, Germany (M.G., E.K.); Department of Pharmacology, Moores Cancer Center, University of California, San Diego, La Jolla, California (J.S.G.)

Received April 27, 2016; accepted July 20, 2016

## ABSTRACT

Frizzleds (FZDs) are unconventional G protein–coupled receptors that belong to the class Frizzled. They are bound and activated by the Wingless/Int-1 lipoglycoprotein (WNT) family of secreted lipoglycoproteins. To date, mechanisms of signal initiation and FZD–G protein coupling remain poorly understood. Previously, we showed that FZD<sub>6</sub> assembles with  $G\alpha_{11}/G\alpha_q$  (but not with  $G\alpha_s$ ,  $G\alpha_o$ , and  $G\alpha_{12/13}$ ), and that these inactive-state complexes are dissociated by WNTs and regulated by the phosphoprotein Dishevelled (DVL). Here, we investigated the inactive-state assembly of heterotrimeric G proteins with FZD<sub>4</sub>, a receptor important in retinal vascular development and frequently mutated in Norrie disease or familial exudative vitreoretinopathy. Live-cell imaging experiments using fluorescence recovery after photobleaching show that human FZD<sub>4</sub> assembles—in a DVL-independent manner—with  $G\alpha_{12/13}$  but not representatives of other heterotrimeric G protein

subfamilies, such as  $G\alpha_{11}$ ,  $G\alpha_o$ ,  $G\alpha_s$ , and  $G\alpha_q$ . The FZD<sub>4</sub>–G protein complex dissociates upon stimulation with WNT-3A, WNT-5A, WNT-7A, and WNT-10B. In addition, WNT-induced dynamic mass redistribution changes in untransfected and, even more so, in FZD<sub>4</sub> green fluorescent protein–transfected cells depend on  $G\alpha_{12/13}$ . Furthermore, expression of FZD<sub>4</sub> and  $G\alpha_{12}$  or  $G\alpha_{13}$  in human embryonic kidney 293 cells induces WNT-dependent membrane recruitment of p115-RHOGEF (RHO guanine nucleotide exchange factor, molecular weight 115 kDa), a direct target of  $G\alpha_{12/13}$  signaling, underlining the functionality of an FZD<sub>4</sub>– $G\alpha_{12/13}$ –RHO signaling axis. In summary,  $G\alpha_{12/13}$ -mediated WNT/FZD<sub>4</sub> signaling through p115-RHOGEF offers an intriguing and previously unappreciated mechanistic link of FZD<sub>4</sub> signaling to cytoskeletal rearrangements and RHO signaling with implications for the regulation of angiogenesis during embryonic and tumor development.

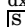
## Introduction

Wingless/Int-1 (WNT)–Frizzled (FZD) signaling is initiated through the interaction of class Frizzled (FZD<sub>1–10</sub>) receptors

The study was financially supported by grants from Karolinska Institutet; Karolinska Institutet's Eye Disease Research Foundation; the Board of Doctoral Education at Karolinska Institutet (J.P., B.H.); the Swedish Research Council [Grants 2011-2435, 2013-5708, and 2015-02899]; the Swedish Cancer Society [Project Grants CAN 2011/690 and CAN 2014/659]; the Knut and Alice Wallenberg Foundation [Grant KAW2008.0149]; the Karolinska Institutet National Institutes of Health Joint PhD Program in Neuroscience (E.A.); the Czech Science Foundation [Grant 13-32990S]; and the Program “KI-MU” [Grant CZ.1.07/2.3.00/20.0180], cofinanced from European Social Fund and the state budget of the Czech Republic and the Marie Curie ITN WntsApp [608180; www.wntsapp.eu]. This research was supported in part by the Intramural Research Program of the National Institutes of Health National Institute of Dental and Craniofacial Research [Grant Z01DE00551]. S.J. was supported by the ERASMUS+ program.

<sup>1</sup>E.A. and B.H. contributed equally to this work.

dx.doi.org/10.1124/mol.116.104919.

 This article has supplemental material available at molpharm.aspetjournals.org.

and their ligands of the WNT family of lipoglycoproteins. WNT signaling holds a central role in embryonic development and the development of human diseases by orchestrating a variety of cellular signaling pathways. The precise mechanisms of signal initiation and specification through WNT binding to the extracellular part of FZD and downstream signal transduction through intracellular signaling partners are so far poorly understood (Nusse, 2003; Angers and Moon, 2009; van Amerongen and Nusse, 2009; Schulte, 2010, 2015; Dijksterhuis et al., 2014).

WNT signaling was historically divided into  $\beta$ -catenin–dependent and -independent pathways.  $\beta$ -Catenin–dependent signals are initiated by WNT binding to FZD and low-density lipoprotein receptor–related protein 5/6 (LRP5/6), recruitment of Dishevelled (DVL), and subsequent inhibition of a destruction complex, resulting in elevated  $\beta$ -catenin levels initiating WNT-target gene transcription (Tamai et al., 2000; Wehrli

**ABBREVIATIONS:** aa, amino acid; C59, 2-[4-(2-methylpyridin-4-yl)phenyl]-N-[4-(pyridin-3-yl)phenyl]acetamide; CL, cross-linking; dcFRAP, double-color fluorescence recovery after photobleaching; DMR, dynamic mass redistribution; DVL, Dishevelled; FRAP, fluorescence recovery after photobleaching; FRET, Förster resonance energy transfer; FZD, Frizzled; GFP, green fluorescent protein; GPCR, G protein–coupled receptor; HEK293, human embryonic kidney 293; Ki16425, 3-(4-(4-((1-(2-chlorophenyl)ethoxy)carbonyl)-3-methylisoxazol-5-yl)benzylthio)propanoic acid; LPA<sub>1</sub>, lysophosphatidic acid 1; pan-DVL, DVL isoforms 1, 2, 3; p115-RHOGEF, RHO guanine nucleotide exchange factor, molecular weight 115 kDa; RGS, regulator of G protein signaling; ROI, region of interest; siRNA, small interfering RNA; WNT, Wingless/Int-1 lipoglycoprotein.

et al., 2000; He et al., 2004; Macdonald et al., 2007; Clevers and Nusse, 2012). Several  $\beta$ -catenin-independent signaling cascades have been described involving small GTPases, such as RHO, RAC, and Cdc42, as well as heterotrimeric G protein signaling through intracellular mobilization of calcium (Semenov et al., 2007; Schulte, 2010). These pathways regulate, for example, cell movement, cytoskeletal reorganization, and planar cell polarity-like signaling in mammalian systems.

Accumulating mechanistic insight strengthens the concept that FZDs behave as bona fide G protein-coupled receptors (GPCRs) (Slusarski et al., 1997; Liu et al., 1999; Sheldahl et al., 1999; Ahumada et al., 2002; Katanaev et al., 2005; Katanaev and Buestorf, 2009; Kilander et al., 2011, 2014a,b; Koval and Katanaev, 2011; Halleskog et al., 2012; Aznar et al., 2015), whereas other aspects, such as G protein coupling selectivity, ligand-dependent functional selectivity, and the importance of G protein signaling downstream of FZDs, still remain obscure (Dijksterhuis et al., 2015).

Heterotrimeric G proteins interact with GPCRs according to distinct dynamic concepts. On one hand, G proteins and receptors assemble in an inactive state, which would explain receptor-G protein selectivity and the rapid responses observed in cells (Oldham and Hamm, 2008). On the other hand, random collision coupling of G protein and receptors is sufficient to form the fully active, agonist-bound receptor conformation inducing release of GDP from  $G\alpha$  and subsequently a rapid GTP-dependent dissociation of the receptor-G protein complex (Neubig, 1994; Hein et al., 2005; Oldham and Hamm, 2008; Rasmussen et al., 2011; Ayoub et al., 2012); both proposed scenarios are supported experimentally (Galés et al., 2005, 2006; Hein et al., 2005; Nobles et al., 2005; Qin et al., 2011). FZD<sub>6</sub> exists in an inactive-state complex with heterotrimeric  $G\alpha_i$  and  $G\alpha_q$  (Kilander et al., 2014b) similar to what was observed for the muscarinic M<sub>3</sub> receptor (Qin et al., 2011). Agonist stimulation of the FZD<sub>6</sub>-G protein complex is followed by rapid dissociation (Kilander et al., 2014b). The FZD isoform, FZD<sub>4</sub>, on which this study focuses has so far not been connected to signaling through heterotrimeric G proteins. FZD<sub>4</sub> signaling, especially in the physiologic context of retinal vascularization, familial exudative vitreoretinopathy, and Norrie disease, is firmly associated with WNT/ $\beta$ -catenin signaling depending on ligand-induced recruitment of LRP5/6 to FZD<sub>4</sub> (Robitaille et al., 2002; Xu et al., 2004; Toomes et al., 2005; Warden et al., 2007; Shastry, 2010). Moreover, it is intriguing that vascularization and angiogenesis, not only limited to the retina, are directly, but independently of each, other linked to FZD<sub>4</sub> and G protein signaling through  $G\alpha_{12/13}$ /RHO signaling (Offermanns et al., 1997; Robitaille et al., 2002; Ye et al., 2009; Sivaraj et al., 2013), suggesting a biologically relevant liaison.

In this study, we set out to investigate the ability of FZD<sub>4</sub> to mediate heterotrimeric G protein signaling. Based on live-cell imaging experiments, we establish that FZD<sub>4</sub> assembles with heterotrimeric  $G\alpha_{12}$  and  $G\alpha_{13}$ , independently of DVL. Stimulation of FZD<sub>4</sub> with WNTs dissociates the receptor-G protein complex, likely leading to G protein activation and subsequent downstream signaling events. We further show that FZD<sub>4</sub> mediates dynamic mass redistribution (DMR) and membrane recruitment of p115-RHOGEF (RHO guanine nucleotide exchange factor, molecular weight 115 kDa), a direct downstream target of active  $G\alpha_{12/13}$ , in a  $G\alpha_{12/13}$ - and WNT-dependent manner. Thus, on the basis of our results, we propose a novel

WNT-FZD<sub>4</sub>- $G\alpha_{12/13}$ -RHO signaling axis offering deeper mechanistic insight into FZD<sub>4</sub> signaling to cytoskeletal rearrangements, RHO signaling, and potentially angiogenesis.

## Materials and Methods

**Cell Culture and Transfections.** Human embryonic kidney 293T (HEK293T) cells (American Type Culture Collection, Manassas, VA) were cultured in Dulbecco's modified Eagle's medium supplemented with 10% fetal bovine serum, 1% penicillin/streptomycin, and 1% L-glutamine (all from Invitrogen, Carlsbad, CA) in a humidified CO<sub>2</sub> incubator at 37°C. Cell culture plastics were from Sarstedt (Nümbrecht, Germany) or Corning Inc. (Corning, NY) unless otherwise specified. For live-cell imaging, immunochemical, and immunoblot analyses, cells were seeded on 35-mm poly-L-lysine-coated or matrigel-coated (1:300 in starvation medium; Sigma-Aldrich, Stockholm, Sweden) glass-bottom dishes (four-chamber 35-mm glass-bottom dishes; Greiner Bio One, Frickenhausen, Germany). Cells were transfected with Lipofectamine 2000 or 3000 according to the manufacturer's instructions (Life Technologies, Carlsbad, CA) 24–48 hours before analysis. To diminish the secretion of endogenously expressed WNTs, cells were pretreated over night with 5  $\mu$ M porcupine inhibitor C59 (2-[4-(2-methylpyridin-4-yl)phenyl]-N-[4-(pyridin-3-yl)phenyl]acetamide; Abcam, Cambridge, UK) where indicated. Recombinant and purified WNT proteins for stimulation experiments were purchased from Bio-Techne/R&D Systems (Minneapolis, MN).

The full-length untagged FZD<sub>4</sub> construct was from www.cdna.org (#FZD400000). Human FZD<sub>4</sub> was subcloned into pEGFP-N1, mCherry-N1, or mCerulean-N1 using NheI and BamHI restriction enzymes. Functionality was assessed by recruitment of DVL from cytosolic punctae to the cell membrane upon coexpression (Supplemental Fig. 1). Green fluorescent protein (GFP)-tagged  $G\alpha_s$  and  $G\alpha_{11}$  were provided by Mark Rasenick (University of Chicago, Chicago, IL) (Yu and Rasenick, 2002);  $G\alpha_q$ -Venus and  $G\alpha_{oA}$ -Venus were from Nevin A. Lambert (Georgia Health Sciences University, Augusta, GA) (Digby et al., 2006); and  $G\alpha_{12/13}$ -mCherry were cloned as an N-terminal fusion to the G protein, according to  $G\alpha_{13}$ -RLucII (Yagi et al., 2011). In detail,  $G\alpha_{13}$ -mCherry was cloned from pCEFL MYC GFP10  $G\alpha_{13}$  wild type (from Silvio Gutkind), introducing a BglII site with forward primer 5' CCAGATCTGCCACCATGGCGGACTTCCTGCCG 3' and an EcoRI site with reverse primer 5' CCGAATTCTCA CTGTAGCATAAGCTGCTT 3'. The  $G\alpha_{13}$  wild type was excised by BglII and EcoRI digest and inserted into pmCherry-C1 vector.  $G\alpha_{12}$ -mCherry was cloned from  $G\alpha_{12}$  EE-tagged (internal; GNA120E100-02 from www.cdna.org) using 5' ATGAATTTCGACCACCATGTCCGGGGTGGT 3' and 5' ATG-GATCCTCACTGCAGCATGATGTCTTCAGGTT 3' to introduce an EcoRI and BamHI site, respectively. The EE-tagged  $G\alpha_{12}$  was excised by EcoRI and BamHI and inserted into pmCherry-C1. Constructs were confirmed by sequencing. Correct membranous localization and activity of the N-terminally tagged  $G\alpha_{12}$ -mCherry and  $G\alpha_{13}$ -mCherry constructs were verified in HEK293 cells. Membranous localization of the mCherry-tagged constructs indicates correct lipidation of the G proteins (Fig. 1; Supplemental Fig. 2 and 3). Further, we used a p115-RHOGEF-GFP recruitment assay in the presence and absence of overexpressed  $G\alpha_{12}$ - and  $G\alpha_{13}$ -mCherry in combination with lysophosphatidic acid 1 receptor (LPA<sub>1</sub> receptor) to further support functionality of the N-terminally tagged G proteins (Supplemental Fig. 2–4). The pCEFL p115-RHOGEF-GFP construct and the extended AU1-tagged regulator of G protein signaling (RGS) domain of p115-RHOGEF (in pCEFL) containing  $G\alpha_{12/13}$ -selective GTPase activating protein/RGS activity were from Silvio Gutkind. The LPA<sub>1</sub> receptor-selective antagonist/inverse agonist Ki16425 (3-(4-(4-((1-(2-chlorophenyl)ethoxy)carbonyl)-3-methylisoxazol-5-yl)benzylthio)propanoic acid) (Ohta et al., 2003; Shano et al., 2008) was able to reduce the LPA<sub>1</sub> receptor-induced membrane recruitment of p115-RHOGEF-GFP, supporting its dependence on endogenously produced agonists or constitutive activity of the LPA<sub>1</sub> receptor upon overexpression

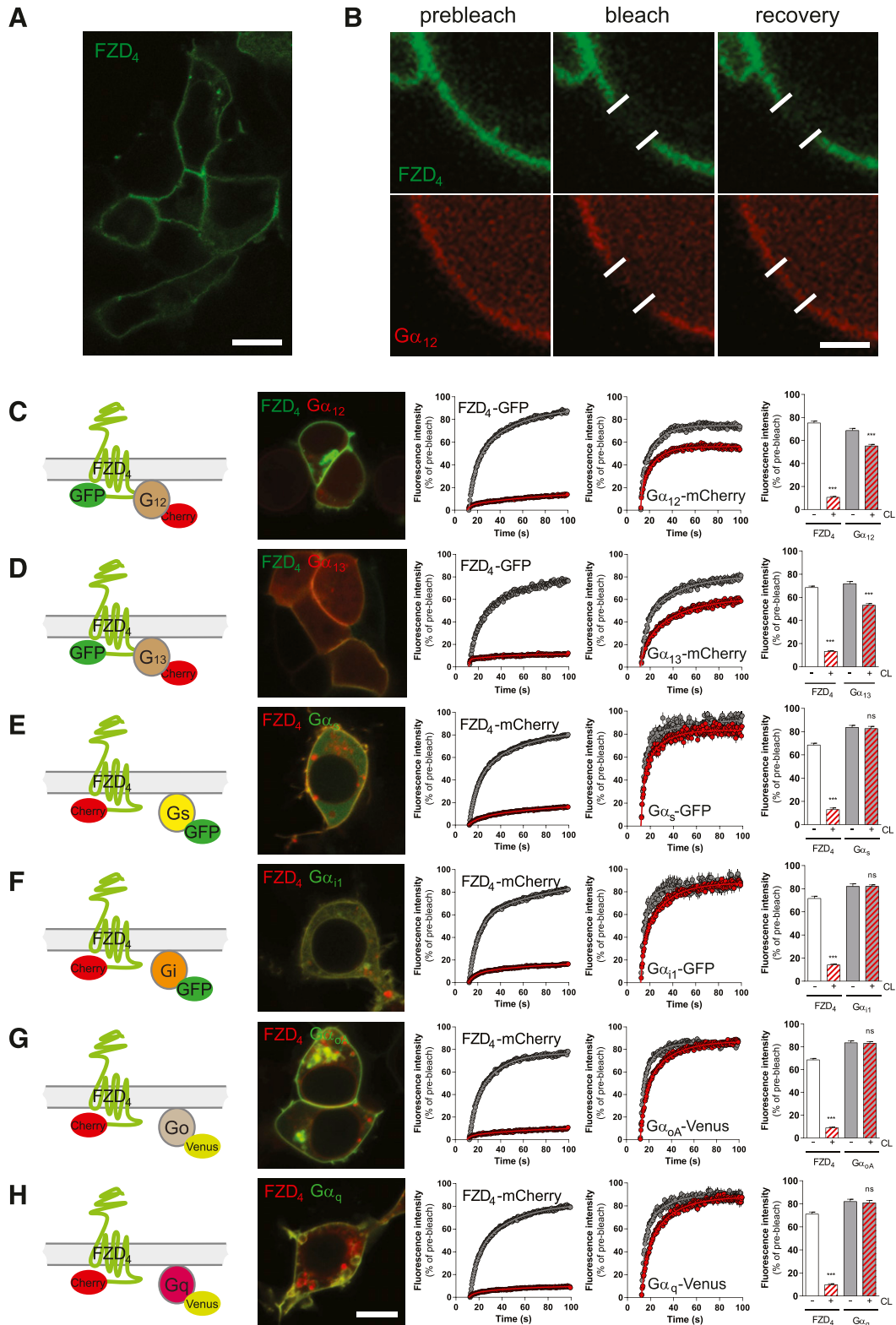


**Fig. 1.** dcFRAP in combination with chemical cell surface crosslinking reveals FZD<sub>4</sub>-G $\alpha_{12/13}$  complex formation. (A) HEK293T cells express fluorescently tagged FZD<sub>4</sub> predominantly in the cell membrane. Size bar = 10  $\mu$ m. (B) dcFRAP experiments are done in cells cotransfected with fluorescently tagged FZD<sub>4</sub>, G $\alpha$  subunits, and untagged  $\beta\gamma$  subunits. Micrographs show FZD<sub>4</sub>-GFP and G $\alpha_{12}$ -mCherry before, shortly after, and about 100 seconds after the high-laser-power photobleaching in a region of interest (white lines). Surface proteins are chemically crosslinked (CL) by Sulfo-NHS-LC-biotin and avidin. Size bar = 2  $\mu$ m. (C–H) The figure includes a schematic presentation clarifying the experimental setup, a confocal micrograph showing HEK293T cells coexpressing FZD<sub>4</sub> with the respective G $\alpha$  subunit (size bar = 10  $\mu$ m), fluorescence intensity curves before (gray) and after (red) CL for both FZD<sub>4</sub> and the respective G protein and a bar graph summarizing the mobile fractions of FZD<sub>4</sub> and the G $\alpha$  subunit under each experimental condition. Color code for mobile fractions (consistent throughout the manuscript): white, FZD<sub>4</sub> before CL; red hatched, FZD<sub>4</sub> after CL; gray, G $\alpha$  before CL; gray + red hatched, G $\alpha$  after CL. \*\*\* $P < 0.001$  ( $n = 3$ ). Error bars provide the S.E.M. ns = not significant.

(Supplemental Fig. 4). The GFP-KRAS fusion protein of the last 25 amino acid (aa) (RKHKEKMSKDGKKKKKSKTKCVIM, including the farnesylation site) of KRAS and the fluorescent protein GFP was provided by Nevin A. Lambert (Lan et al., 2011). FLAG-epitope-tagged DVL1 was from Madelon M. Maurice (University Medical Center, Utrecht, The Netherlands), DVL2-MYC was from S. A. Yanagawa (Kyoto University, Kyoto, Japan), and DVL3-FLAG was from Randall T. Moon (University of Washington School of Medicine, Seattle, WA). All constructs were confirmed by sequencing.

For human DVL silencing, DVL 1, 2, 3 (panDVL) small interfering RNA (siRNA; AAGUCAACAAGAUCACCUUCU) targeting position 1450–1468 of human DVL1, isoform 1; position 1375–1393 of human DVL1, isoform 2; position 1474–1492 of DVL2; and position 1441–1459 of DVL3 or Xeragon (Qiagen, Sollentuna, Sweden) control nonsilencing siRNA (AAUUCUCCGAACGUGUCACGU) was added simultaneously with plasmids (Bryja et al., 2008). Cells were transfected at a 3:1:1:1 ratio of receptor: $G\alpha$ : $\beta$ : $\gamma$  plasmids or at a 3:1 ratio of receptor:DVL plasmids.

#### Dual-Color Fluorescence Recovery after Photobleaching.

The procedure was essentially as described in Kilander et al. (2014b), Qin et al. (2011), and Qin et al. (2008). Cells were grown on 35-mm extracellular matrix; coated (1:300; Sigma-Aldrich) glass-bottom dishes and assessed using a Zeiss 710 laser-scanning microscope (Zeiss, Jena, Germany). Membranous, tagged FZD<sub>4</sub> was immobilized using avidin-biotin cross-linking. In brief, cells were incubated 0.5 mg/ml NHS-sulfo-LC-LC-biotin followed by 0.1 mg/ml avidin (Thermo Fisher Scientific, Stockholm, Sweden) for 15 minutes each at room temperature and rinsed three times before, between, and after incubations. Washing and incubation steps were performed in cross-linking (CL) buffer (150 mM NaCl, 2.5 mM KCl, 10 mM HEPES, 12 mM glucose, 0.5 mM CaCl<sub>2</sub>, and 0.5 mM MgCl<sub>2</sub>, adjusted to pH 8.0). Cellular imaging was performed within 1 hour of avidin exposure. Measurements in which the receptor's mobility was not sufficiently affected by CL were excluded [cutoff:  $\geq 40\%$  fluorescence recovery after photobleaching (FRAP) recovery]. Images were acquired using a 40 $\times$ , 1.2 numerical aperture C-Apochromat objective (Zeiss), and the 488- and 561-nm laser lines were used to excite GFP-Venus and mCherry fluorophores, respectively. For all FZD<sub>4</sub>- $G\alpha$  subunit combinations, untagged  $\beta\gamma$  subunits were cotransfected. For FRAP experiments, a 2.86  $\times$  2.86- $\mu\text{m}$  defined area was placed over the cell plasma membrane and monitored using low-intensity illumination. Care was taken to select cells that appeared to have more receptor than G protein expressed, taking into account laser power and gain settings and the differences in the fluorescence yield of the fluorescent proteins. After an initial prebleach period, irreversible photobleaching was performed by increasing the laser intensity to 100%. Fluorescent recovery after bleaching was measured using low illumination again, and was measured for a total of 101 seconds. Average pixel intensity was recorded using the ZEN2013 software (Zeiss), corrected for photobleaching and background fluctuations, and normalized to prebleached intensity. The mobile fraction ( $F_m$ ) was calculated as  $F_m = (I_P - I_0) / (I_1 - I_0)$ , where  $I_1$  is the initial intensity measured before bleaching,  $I_0$  is the immediate fluorescence intensity after bleaching, and  $I_P$  is the intensity value after recovery of fluorescence. The mobile fraction was determined by averaging fluorescence intensity values obtained between 55 and 85 seconds.

**Förster Resonance Energy Transfer-Photoacceptor Bleaching.** HEK293 cells were seeded on sterile, gelatin-coated coverslips in a 24-well plate and transfected with FZD<sub>4</sub>-GFP, untagged  $\beta\gamma$ , and  $G\alpha_{12}$ - or  $G\alpha_{13}$ -mCherry subunits. The cells were treated with or without WNT-7A (300 ng/ml; 5 minutes) prior to fixation in 4% paraformaldehyde. Förster resonance energy transfer (FRET) between FZD<sub>4</sub>-GFP and  $G\alpha_{12}$ - or  $G\alpha_{13}$ -mCherry subunits was performed on an LSM710 (Zeiss), with a 40 $\times$  water-immersion objective (C-Apochromat, 1.2 numerical aperture; Zeiss) by acceptor photobleaching with 100% laser power of a 561-nm diode laser for 20 seconds. Signal intensity of the photoacceptor (mCherry) was routinely reduced by 80–90%. Images were acquired before and after

photobleaching with excitation/emission ranges of 488/493–545 nm (GFP) and 561/562–681 nm (mCherry). Quantification of the GFP emission before and after the photobleaching was determined with region of interest (ROI) analysis in at least 10 individual cells per experiment and condition using the ZEN2013 software. Data were background corrected and adjusted for fluctuations in intensity with an unbleached ROI as reference. FRET efficiency was calculated as  $E = [1 - (I_{pre}/I_{post})] \times 100\%$ . Control experiments were performed using FZD<sub>4</sub>-GFP and myristoylated mCherry to define basal FRET of fluorescent proteins coexpressed in the same cellular compartment.

**Dynamic Mass Redistribution.** Label-free measurements were performed using the Epic System (Corning) as described previously in detail (Schröder et al., 2011; Grundmann and Kostenis, 2015). In brief, HEK293 cells were seeded onto fibronectin-coated 384-well biosensor plates at a density of 15,000 cells per well in complete growth medium. After 4 hours, the medium was exchanged for starvation medium lacking fetal bovine serum but supplemented with 5  $\mu\text{M}$  porcupine inhibitor C59 and incubated at 37°C overnight. Cells were washed with Hanks' balanced salt solution containing 20 mM HEPES, 5  $\mu\text{M}$  C59, and equilibrated at 37°C for at least 1 hour before compound addition and DMR recording. Experiments were performed 24–48 hours after transfection of pcDNA3.1(+) or FZD<sub>4</sub>-pEGFP-N1 using FuGENE HD (Promega, Madison, WI). HEK293 cells lacking  $G\alpha_{12/13}$  were a kind gift from Dr. Asuka Inoue (Tohoku University, Sendai City, Japan).  $G\alpha_{12/13}$ , which are encoded by the GNA12 and the GNA13 genes, respectively, were simultaneously targeted by a CRISPR-Cas9 system.

**p115-RHOGEF-GFP Recruitment Assay.** HEK293 cells were seeded onto four-chamber glass-bottom dishes (coated with extracellular matrix gel 1:300; Sigma-Aldrich) and transfected with combinations of FZD<sub>4</sub>-Cerulean,  $G\alpha_{12}$ - or  $G\alpha_{13}$ -mCherry, p115-RHOGEF-GFP, and untagged  $\beta\gamma$  subunits (ratio 3:1:1:1:1). The next day, the living cells were examined by confocal microscopy (Zeiss LSM510; C-Apochromat 40 $\times$ /1.2W) to visualize the fluorescently tagged proteins using sequential scanning in combination with 405-nm excitation/420–480 nm emission, 488 nm/long pass 505 nm, and 543 nm/LP 560 nm for Cerulean, GFP, and mCherry, respectively. Cross-talk/bleed-through was controlled using cells expressing the single fluorescent proteins. The Zeiss ZEN2013 software was used to generate fluorescence intensity profiles. For quantification of p115-RHOGEF-GFP membrane recruitment, random images were taken at higher magnification. Cell categories “membranous” and “cytosolic” were defined for p115-RHOGEF-GFP distribution and more than 50 (up to several hundred) cells per condition (+/- FZD<sub>4</sub>-Cerulean) were counted from three independent experiments. Data are presented as a percentage of all counted p115-RHOGEF-GFP-positive cells showing membranous p115-RHOGEF-GFP distribution.

**Western Blot Analysis.** HEK293T cells were plated in a 24-well plate at a density of 150,000 cells/well and grown overnight. Cells were transfected using Lipofectamine 2000 or 3000 according to the manufacturer's instructions. For lysis, equal amounts of a 2 $\times$  SDS sample buffer were applied to the cells. Protein lysates were analyzed by standard SDS-PAGE/immunoblotting using the following primary antibodies: mouse anti- $\beta$ -actin (1:30,000; Sigma-Aldrich), mouse anti-DVL1 (1:500; Santa Cruz Biotechnology, Dallas, TX), rabbit anti-DVL2 (1:1000; Cell Signaling Technology, Danvers, MA), mouse anti-DVL3 (1:500; Santa Cruz), mouse anti-MYC (1:500; Santa Cruz Biotechnology), and mouse anti-FLAG M2 (1:1000; Sigma-Aldrich). Signals were detected by horseradish peroxidase-conjugated secondary antibodies (Thermo Fisher Scientific) and visualized with standard enhanced chemiluminescence detection protocols.

**Statistical Analysis.** Statistical and graphical analyses were performed using GraphPad Prism 6 software (GraphPad Software, La Jolla, CA). FRAP data were analyzed by one-way analysis of variance/post hoc Bonferroni's multiple comparisons or Student's *t* test. Curve fitting of FRAP data was achieved with a two-phase association nonlinear function using the least-squares fit. All experiments were repeated at least three times; FRAP data were based on

8–55 ROIs per data point from at least three independent experiments. The number of ROIs per data point varies because some ROIs are excluded from the analysis, such as when visual inspection indicated that cellular movements led to a repositioning of the observed bleached membrane area from the ROI during the recovery phase after photobleaching. The analyzed ROIs originated from individual cells from independent cell transfections. Significance levels are given as follows: \* $p < 0.05$ , \*\* $p < 0.01$ , and \*\*\* $p < 0.001$ . Data in FRAP curves and FRAP bar graphs are presented as the mean  $\pm$  S.E.M. Quantitative assessment of protein translocation (DVL1-FLAG and p115-RHOGEF-GFP) was done by manual counting by an observer blinded to the experimental conditions. At least 50 cells in total were counted per experimental condition in three independent experiments. Results are presented in bar graphs as means  $\pm$  S.E.M. Statistics were done by a one-way analysis of variance with Tukey test for multiple comparisons.

## Results

**FZD<sub>4</sub> Interacts with the Heterotrimeric G Proteins G $\alpha_{12}$  and G $\alpha_{13}$  but Not G $\alpha_{11}$ , G $\alpha_o$ , G $\alpha_s$ , G $\alpha_q$ .** To assess the ability of FZD<sub>4</sub> to assemble with heterotrimeric G proteins in an inactive-state complex, we expressed FZD<sub>4</sub>-GFP or FZD<sub>4</sub>-mCherry in HEK293T cells. Both constructs showed membrane localization and were able to recruit DVL from a distinct punctuate pattern of cytosolic aggregates to the plasma membrane, similar to the full-length, untagged human FZD<sub>4</sub> (Supplemental Fig. 1). Upon coexpression in HEK293T cells, FZD<sub>4</sub> colocalized with fluorescently labeled G $\alpha_{11}$ , G $\alpha_o$ , G $\alpha_s$ , G $\alpha_q$ , G $\alpha_{12}$ , and G $\alpha_{13}$  subunits predominantly in the plasma membrane (Fig.

1). To assess FZD<sub>4</sub>-G protein interaction, we took advantage of a dual-color FRAP (dcFRAP) protocol that enables simultaneous assessment of lateral mobility of two fluorescently tagged proteins (Phair et al., 2004; Qin et al., 2008, 2011; Dorsch et al., 2009; Kilander et al., 2014b) (Fig. 1). This experimental setup is based on immobilization of transmembrane proteins by chemical surface CL with sulfo-NHS-LC-LC-biotin and avidin. In contrast to transmembrane receptors, intracellular proteins, such as the heterotrimeric G proteins, are not directly affected by surface CL in this assay. The mobile fraction of intracellular proteins is reduced only upon interaction with CL-immobilized surface proteins (Qin et al., 2008, 2011; Kilander et al., 2014b). In cells transfected with fluorescently tagged FZD<sub>4</sub>, G $\alpha$ , and untagged  $\beta\gamma$ , we found that the mobile fraction of FZD<sub>4</sub> was remarkably reduced by surface cross-linking (Fig. 1, C–H). In accordance with an inactive-state assembly of receptor and G protein, we found that the mobile fraction of G $\alpha_{12}$  and G $\alpha_{13}$ , but not that of other representatives of the G protein subfamilies (G $\alpha_s$ , G $\alpha_{i/o}$ , and G $\alpha_q$ ), was affected by surface cross-linking of the receptor (Fig. 1, C–H). To verify that these observed effects were selectively dependent on FZD<sub>4</sub> coexpression, and to control for general effects of surface CL on G protein mobility, we previously performed dcFRAP experiments with myristoylated fluorescent proteins as nonreceptor control in combination with fluorescently tagged heterotrimeric G $\alpha_i$  proteins (Kilander et al., 2014b). In Fig. 2, we show that chemical surface cross-linking in the absence of overexpressed FZD<sub>4</sub> but in the presence of a membrane-anchored fluorescent protein (GFP-KRAS) did not affect lateral mobility of the

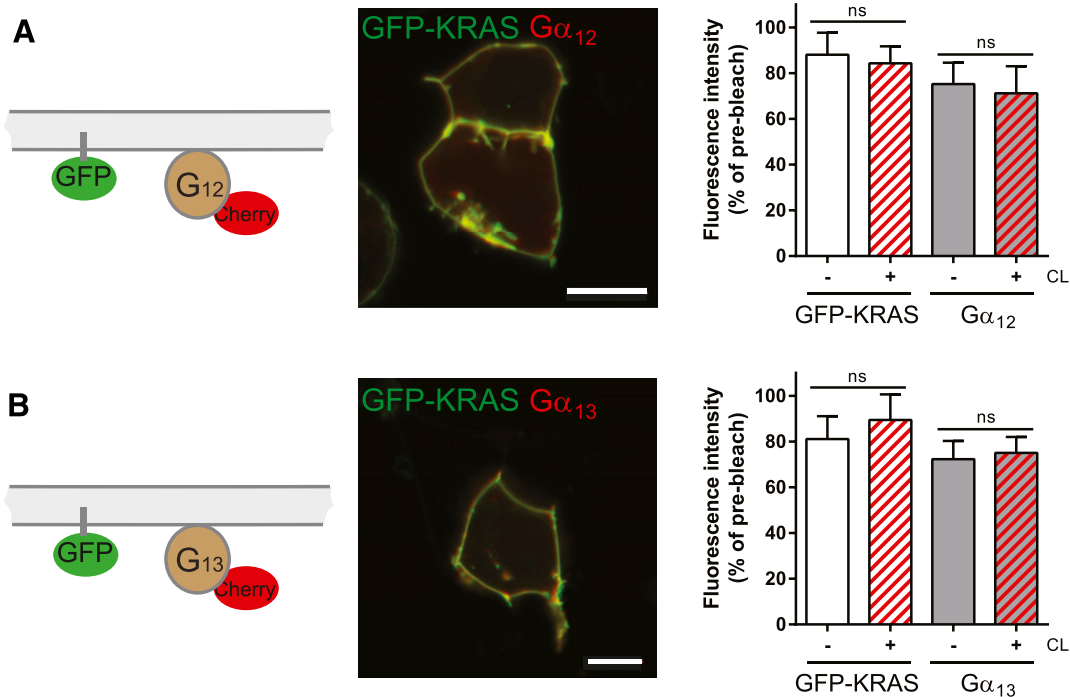


**Fig. 2.** Nonreceptor control ensures that the mobile fraction of G $\alpha_{12/13}$ -mCherry is not affected by chemical surface crosslinking in the absence of FZD<sub>4</sub>. HEK293 cells expressing farnesylated GFP-KRAS, untagged  $\beta\gamma$  subunits, and N-terminally tagged G $\alpha_{12}$ -mCherry were used for a dcFRAP assay using chemical surface crosslinking (CL) with Sulfo-NHS-LC-LC-biotin and avidin as described in Fig. 1. CL affected neither the mobile fraction of GFP-KRAS nor that of G $\alpha_{12}$ -mCherry (A) or G $\alpha_{13}$ -mCherry (B). The figure includes a schematic presentation clarifying the experimental setup, a confocal micrograph showing HEK293T cells coexpressing GFP-KRAS with the G $\alpha_{12}$ -mCherry (A) or G $\alpha_{13}$ -mCherry (B; size bars = 10  $\mu$ m), fluorescence intensity curves before (gray) and after (red) CL for both GFP-KRAS and G $\alpha_{12/13}$ -mCherry, and a bar graph summarizing the mobile fractions of GFP-KRAS and the G $\alpha$  subunit under each experimental condition. The data verify that the decrease in G protein mobile fraction observed for G $\alpha_{12/13}$ -mCherry in the presence of FZD<sub>4</sub>-GFP is not evoked by CL of endogenously expressed receptors. Error bars provide the S.E.M. ns, not significant. \*\*\* $P < 0.001$ . Bar graph summarizes measurements from at least four independent experiments, each including data from several individual cells.



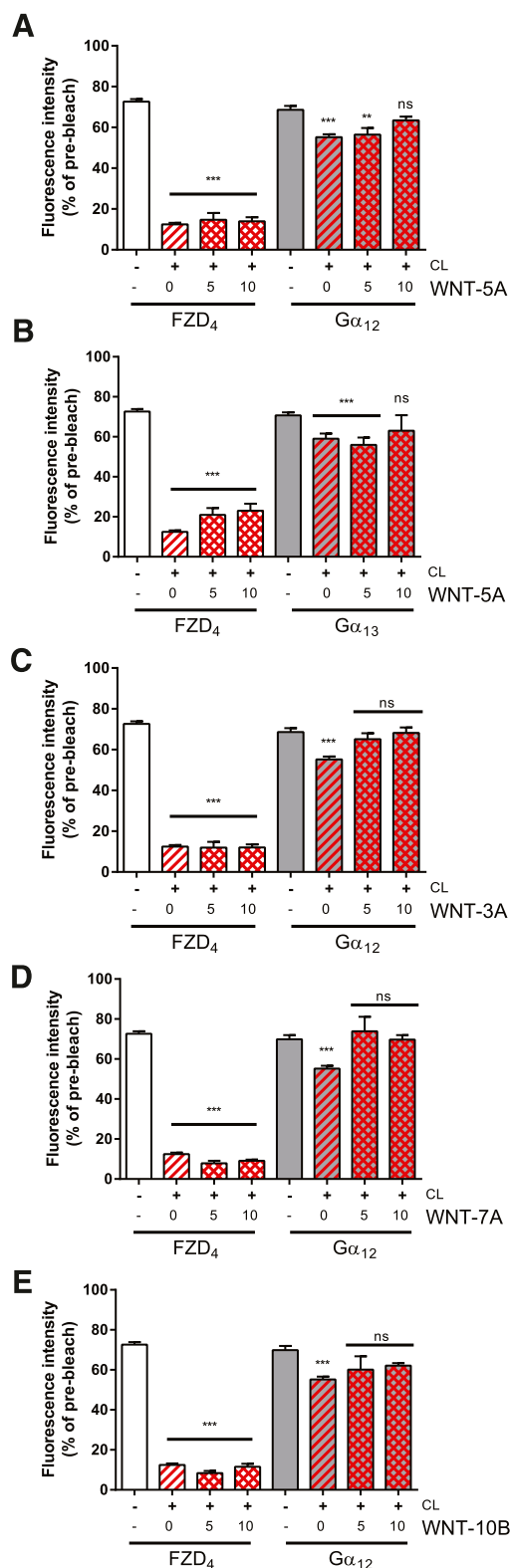


**Fig. 3.** FZD<sub>4</sub>-Gα<sub>12/13</sub> complex dissociates upon WNT stimulation. dcFRAP experiments were performed in HEK293T cells expressing FZD<sub>4</sub>-GFP and Gα<sub>12</sub>- or Gα<sub>13</sub>-mCherry. The mobile fractions of the two proteins were determined before and after CL, as well as 5 and 10 minutes after CL/WNT stimulation (all WNTs at 300 ng/ml). Kinetic analysis of the mobile fraction indicates dissociation of the receptor G protein complex upon WNT stimulation. (A and B) For WNT-5A, we investigated WNT-induced dissociation from FZD<sub>4</sub>-GFP for Gα<sub>12</sub>- or Gα<sub>13</sub>-mCherry. (C–E) For the other WNTs (WNT-3A, -7A, 10B), only WNT-induced Gα<sub>12</sub>-mCherry dissociation was measured. \**P* < 0.05; \*\**P* < 0.01; \*\*\**P* < 0.001 (*n* = 3).

heterotrimeric Gα<sub>12</sub>-mCherry and Gα<sub>13</sub>-mCherry proteins in the presence of untagged βγ, indicating that cross-linking of endogenously expressed receptors does not perturb the interpretation of our data. This observation is further supported by the finding that the mobile fraction of Gα<sub>12</sub>-mCherry in the presence of FZD<sub>6</sub>-GFP is not affected by CL (Kilander et al., 2014b), indicating that even chemical immobilization of an overexpressed transmembrane protein that does not interact with the heterotrimeric G protein leaves the mobile fraction of the G protein unchanged.

**The FZD<sub>4</sub>-Gα<sub>12/13</sub> Complex Dissociates upon WNT Stimulation.** With the purpose of determining whether agonist treatment disrupts the observed FZD<sub>4</sub>-Gα<sub>12/13</sub> complex, we stimulated HEK293T cells expressing FZD<sub>4</sub>-GFP, untagged βγ, and Gα<sub>12/13</sub>-mCherry with commercially available, purified WNTs (300 ng/ml; 0, 5, 10 minutes; Fig. 3). As expected from earlier experiments with FZD<sub>6</sub> and Gα<sub>11</sub> or Gα<sub>q</sub> proteins (Kilander et al., 2014b), the previously observed CL-induced reduction of the mobile fraction of the Gα<sub>12/13</sub> proteins was abolished by WNT-3A, -5A, -7A, and -10B treatment, indicating dissociation of the inactive-state FZD<sub>4</sub>-GFP/Gα<sub>12/13</sub>-mCherry complex. To further support the dcFRAP data on agonist-induced complex dissociation, we used FRET measurements in fixed HEK293 cells transfected with FZD<sub>4</sub>-GFP, untagged βγ, and Gα<sub>12/13</sub>-mCherry. Photo-acceptor bleaching FRET measurements indicated that energy transfer from FZD<sub>4</sub>-GFP to Gα<sub>12/13</sub>-mCherry occurred at baseline, and that FRET decreased with WNT-7A stimulation (300 ng/ml; 5 minutes; Fig. 4), indicative of a receptor-G protein dissociation or rearrangement, similar to what was previously observed in the case of FZD<sub>6</sub> and Gα<sub>11</sub> or Gα<sub>q</sub> (Kilander et al., 2014b). The negative control coexpressing FZD<sub>4</sub>-GFP and myristoylated mCherry defines background levels of basal FRET between fluorescent proteins that are coexpressed in the same cellular compartment but only randomly approaching each other to yield FRET. Importantly, WNT-7A stimulation reduced FRET between FZD<sub>4</sub>-GFP and Gα<sub>12/13</sub>-mCherry to basal levels resembling those of the negative control. Thus, both the affinity-based dcFRAP assay and the proximity-based FRET assay support FZD<sub>4</sub>-G protein interaction and agonist-induced dissociation.

**The FZD<sub>4</sub>-Gα<sub>12/13</sub> Complex Is Independent of DVL.** Since we previously identified DVL as a master regulator of FZD<sub>6</sub>-Gα<sub>11</sub> or FZD<sub>6</sub>-Gα<sub>q</sub> association (Kilander et al., 2014b), we also investigated the role of the scaffold protein DVL in the formation of the inactive-state assembled complex between FZD<sub>4</sub> and Gα<sub>12/13</sub> by in vitro loss- and gain-of-function experiments. On one hand, we overexpressed DVL1, DVL2, and DVL3 in HEK293T cells expressing FZD<sub>4</sub> and Gα<sub>12</sub>-mCherry and untagged βγ subunits at a plasmid ratio of 3:1:1 receptor:Gαβγ:DVL. On the other hand, we downregulated DVL1, DVL2, and DVL3 using pan-DVL siRNA designed to target all three human isoforms of DVL (Fig. 5). Thereby, we created cellular systems with low (pan-DVL siRNA), intermediate (endogenous), and high DVL levels (DVL overexpression). When performing dcFRAP experiments in these cellular setups, we found that changed DVL expression levels did not affect FZD<sub>4</sub>-Gα<sub>12</sub> complex formation (Fig. 5), indicating

Error bars provide the S.E.M. ns, not significant. Bar graph summarizes measurements from at least three independent experiments, each including data from several individual cells.

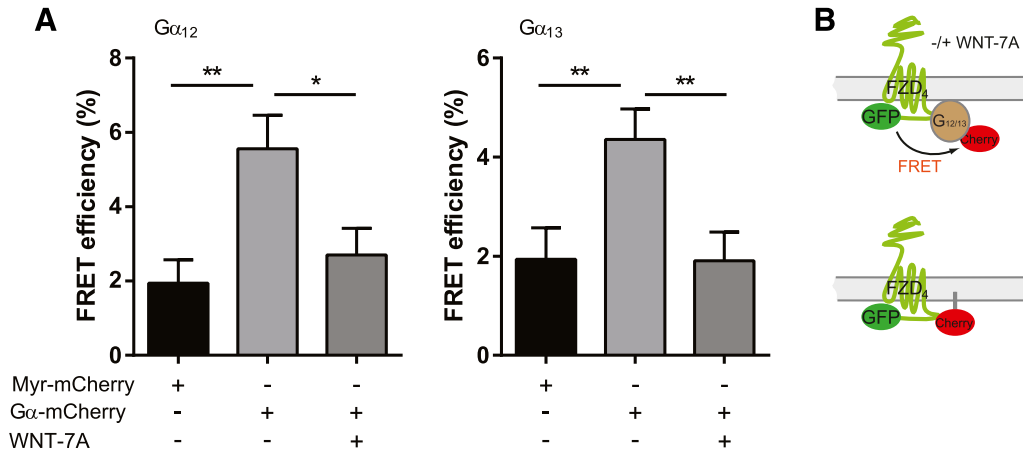


**Fig. 4.** FRET analysis supports WNT-evoked FZD<sub>4</sub>-G $\alpha_{12/13}$  complex dissociation. (A) FRET analysis performed in HEK293 cells expressing FZD<sub>4</sub>-GFP, untagged  $\beta\gamma$  subunits, and either G $\alpha_{12}$ - or G $\alpha_{13}$ -mCherry indicates that FRET between GFP and mCherry decreased in response to WNT-7A stimulation (300 ng/ml; 5 minutes). FRET measurements were performed with photoacceptor bleaching in fixed cells. Light grey bars show FRET between GFP and mCherry in the absence of WNT stimulation. Dark grey bars show FRET upon WNT stimulation. Black bars show FRET efficiency at baseline in cells expressing myristoylated mCherry as negative control. The bar graph summarizes data from three independent experiments with a minimum of 27 ROIs from different cells analyzed per individual experiment and condition. Bars and error bars provide the mean  $\pm$  S.E.M., respectively. \* $P < 0.05$ ; \*\* $P < 0.001$ . (B) The experimental setup is illustrated schematically.

that the scaffold protein DVL is not required and is dispensable for WNT-FZD<sub>4</sub>-G $\alpha_{12/13}$  inactive-state complex formation.

**Analysis of G Protein Selectivity of FZD<sub>4</sub> and FZD<sub>6</sub> Chimeric Receptors.** Given that prediction of receptor G protein selectivity from the primary GPCR structure is still

not possible, we aimed to combine our knowledge from FZD<sub>6</sub> as a receptor selectively interacting with G $\alpha_i$  and G $\alpha_q$  and FZD<sub>4</sub> as a receptor that assembles with G $\alpha_{12/13}$  to shed light on domains required for G protein selectivity in FZDs. Both receptors belong to different homology clusters grouping

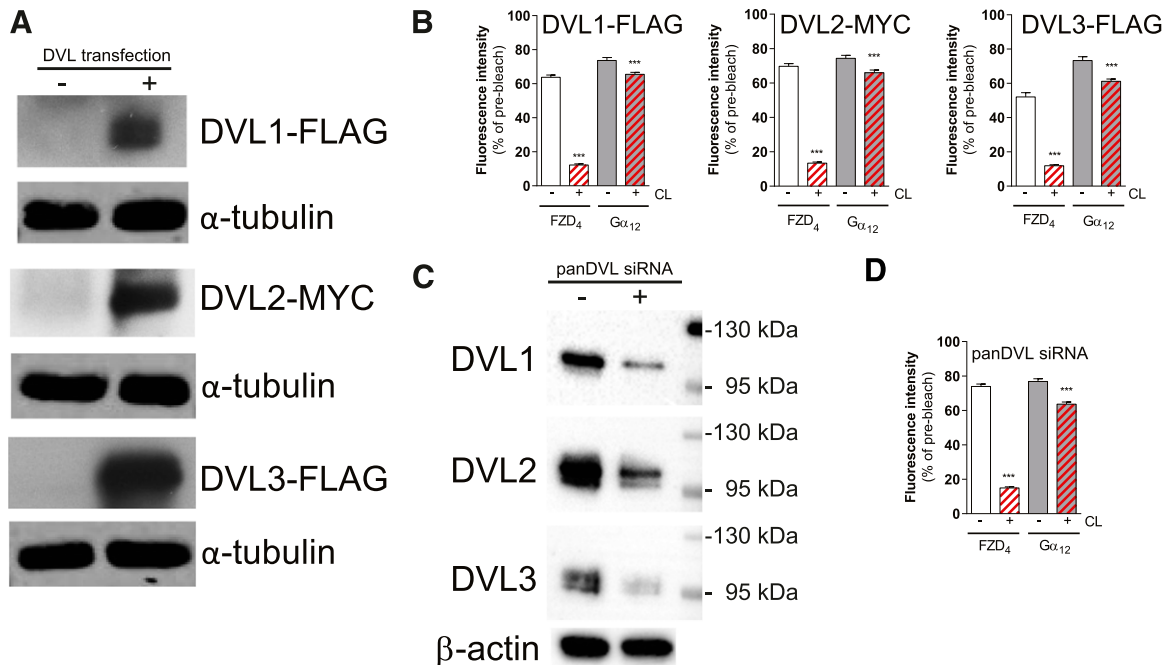


**Fig. 5.** DVL does not play a central role for FZD<sub>4</sub>-G $\alpha_{12/13}$  complex formation. (A and B) DVL1-FLAG, DVL2-MYC, and DVL3-FLAG were coexpressed in HEK293T cells. Cells that were used for dcFRAP were lysed afterward to assess DVL1, DVL2, and DVL3 levels in cellular lysates by immunoblotting using anti-FLAG or anti-MYC antibodies.  $\alpha$ -Tubulin was used as the loading control. (B) dcFRAP experiments in cells coexpressing FZD<sub>4</sub>-GFP and G $\alpha_{12}$ -mCherry in the presence of DVL1, DVL2, or DVL3. Downregulation of DVL1, DVL2, and DVL3 by using pan-DVL siRNA did not affect FZD<sub>4</sub>-G $\alpha_{12/13}$  assembly. Bar graphs summarize dcFRAP measurements from three independent experiments, each including data from several individual cells. Densitometry analysis of three independent experiments using panDVL siRNA and control indicated that DVL1, DVL2, and DVL3 were routinely reduced by 35–56% [values in percentage reduction in DVL1, DVL2, and DVL3 band intensity by panDVL siRNA compared with control siRNA (mean  $\pm$  S.E.M.): DVL1 (40  $\pm$  8%); DVL2 (56  $\pm$  2%); DVL3 (35  $\pm$  4%)]. For a graphical presentation of the DVL1, DVL2, and DVL3 levels in control and panDVL siRNA-treated cells ( $N = 3$ ), see Supplemental Fig. 6. (C) Immunoblotting indicates reduced expression of the three endogenous DVL isoforms in HEK293T cells used for dcFRAP. (D) dcFRAP analysis in cells coexpressing FZD<sub>4</sub>-GFP and G $\alpha_{12}$ -mCherry shows no change in the mobile fraction of G $\alpha_{12}$ -mCherry upon CL in cells with reduced levels of DVL. \*\*\* $P < 0.001$  ( $n = 3$ ). Error bars provide the S.E.M. Bar graphs summarize measurements from three independent experiments, each including data from several individual cells.



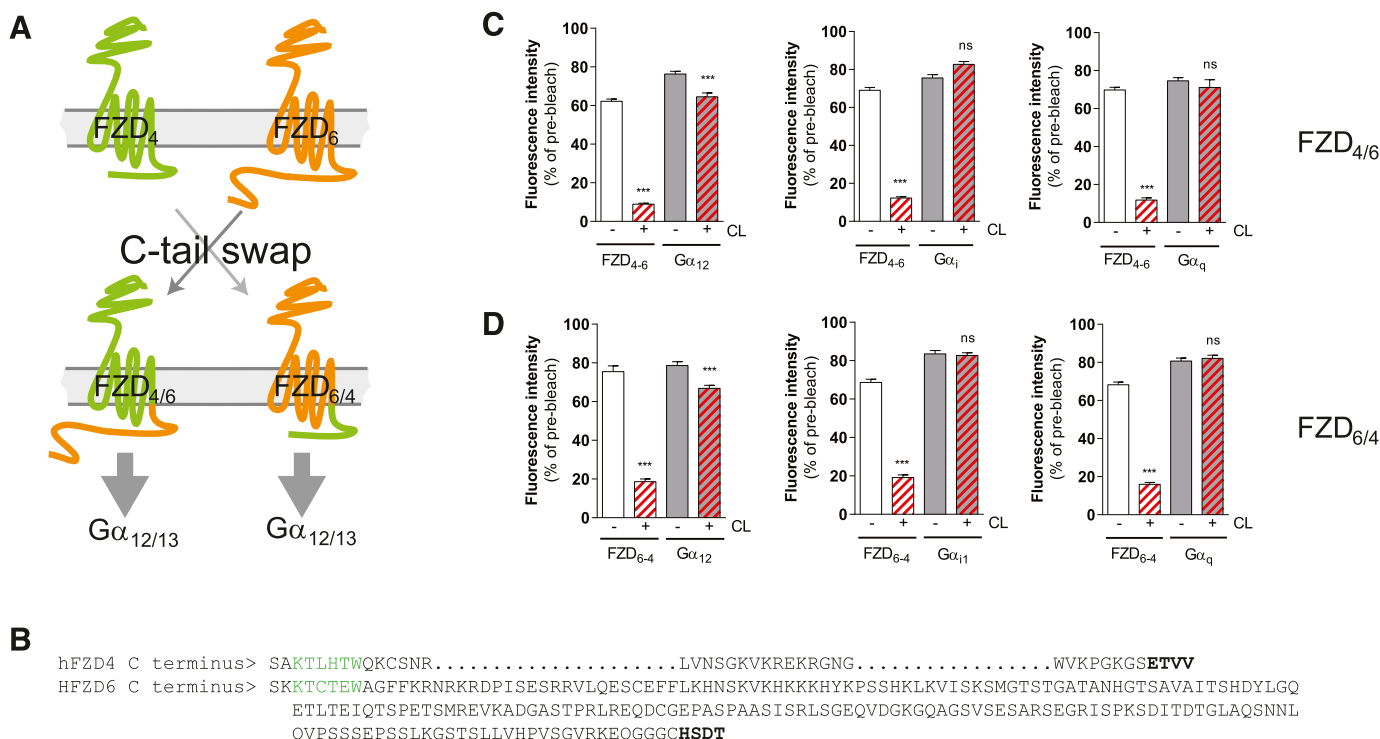


**Fig. 6.** C-terminal domain swapping between FZD<sub>4</sub> and FZD<sub>6</sub>. (A) Schematic presentation of the exchange strategy of the C termini between FZD<sub>4</sub> and FZD<sub>6</sub>, resulting in FZD<sub>4-6</sub> C-terminal tail and FZD<sub>6-4</sub> C-terminal tail. (B) The primary structure of human FZD<sub>4</sub> and FZD<sub>6</sub>. Green highlights the conserved KTxxxW sequence involved in DVL binding on the presumptive helix 8. Bold marks the terminal PDZ ligand domain. dcFRAP experiments in HEK293T cells coexpressing FZD<sub>4-6</sub>-GFP and Gα<sub>12</sub>-mCherry, FZD<sub>4-6</sub>-mCherry and Gα<sub>11</sub>-GFP, or FZD<sub>4-6</sub>-mCherry and Gα<sub>q</sub>-Venus (C) and FZD<sub>6-4</sub>-GFP and Gα<sub>12</sub>-mCherry, FZD<sub>6-4</sub>-mCherry and Gα<sub>11</sub>-GFP, or FZD<sub>6-4</sub>-mCherry and Gα<sub>q</sub>-Venus (D) reveal predominant assembly with Gα<sub>12</sub> of the chimeric receptors. \*\*\**P* < 0.001 (*n* = 3). Bar graphs show the mean ± S.E.M. PDZ, PSD-95/dics large/ZO-1 homologous.

FZD<sub>4,9,10</sub> and FZD<sub>3,6</sub> (Schulte, 2010), and their C termini differ dramatically in length: the FZD<sub>4</sub> C tail comprises 41 aa, and the FZD<sub>6</sub> tail consists of 211 aa. The hypothesis for creating FZD<sub>4</sub>-FZD<sub>6</sub> tail and FZD<sub>6</sub>-FZD<sub>4</sub> tail chimera through a classic domain swap of the C-terminal regions was that exchanging C-terminal tails could be accompanied by interchanging G protein selectivity. In Fig. 6, C and D, dcFRAP data are shown, indicating G protein selectivity of the respective chimera. Whereas the G protein-coupling selectivity of the FZD<sub>6</sub>-FZD<sub>4</sub> tail chimera was switched from Gα<sub>1</sub>/Gα<sub>q</sub> to Gα<sub>12</sub>, the FZD<sub>4</sub>-FZD<sub>6</sub> tail chimera still preferentially bound to Gα<sub>12</sub> rather than Gα<sub>1</sub> or Gα<sub>q</sub>.

**WNT-Induced Dynamic Mass Redistribution in HEK293 Depends on Gα<sub>12/13</sub>.** Recent developments in label-free technologies, such as DMR measurements, allow global analysis of ligand-induced changes in living cells (Schröder et al., 2011; Grundmann and Kostenis, 2015). DMR in living cells presents a holistic view on changes in multiple cellular processes, such as protein trafficking, morphologic changes, cytoskeletal rearrangement, receptor internalization, or adhesion (Schröder et al., 2010), some of which are connected to Gα<sub>12/13</sub> signaling (Worzfeld et al., 2008). To investigate whether DMR technology is competent to visualize the cellular consequences set in motion by WNT-5A upon activation of FZD<sub>4</sub>-Gα<sub>12/13</sub> complexes, we used HEK293 cells genetically deficient or not deficient in Gα<sub>12/13</sub> and monitored WNT-induced alterations of global cell activity. We observed negative DMR upon stimulation with WNT-5A in vector-transfected HEK293 wild-type cells (Fig. 7A), indicating interaction of WNT-5A with a molecular target

endogenous to the HEK293 cell background. Importantly, overexpression of FZD<sub>4</sub>-GFP intensified this response, which substantiates a FZD<sub>4</sub> receptor-dependent WNT-5A mode-of-action (Fig. 7B). Strikingly, these responses were completely sensitive to Gα<sub>12/13</sub> protein knockout (Fig. 7, C and D), indicative of FZD<sub>4</sub> receptor signaling via Gα<sub>12/13</sub>. FZD<sub>4</sub> receptor-independent cell responses induced by the direct adenylate cyclase stimulator forskolin, however, remained unaffected by either Gα<sub>12/13</sub> protein knockout or FZD<sub>4</sub>-GFP overexpression (Supplemental Fig. 5).

**Signaling along a WNT-FZD<sub>4</sub>-Gα<sub>12/13</sub>-p115-RHOGEF Signaling Axis.** To link the FZD<sub>4</sub>-Gα<sub>12/13</sub> complex functionally to downstream signaling events, and to support the idea that FZD<sub>4</sub> indeed mediates the GDP/GTP exchange at Gα<sub>12/13</sub> proteins, we expanded on previous findings identifying p115-RHOGEF as a Gα<sub>12/13</sub> target that physically interacts with the active, GTP-bound α subunit and stimulates its GTPase activity similar to classic regulators of G protein signaling proteins (Hart et al., 1996, 1998; Meyer et al., 2008; Worzfeld et al., 2008). Most importantly, with regard to the functionality of the tagged Gα<sub>12/13</sub>-mCherry subunits, correct palmitoylation of Gα<sub>12/13</sub> is required for the G protein's plasma membrane localization and the promotion of p115-RHOGEF recruitment to the plasma membrane by the active, GTP-bound G protein (Bhattacharyya and Wedegaertner, 2000). Comparable to the results with coexpression of the LPA<sub>1</sub> receptor and Gα<sub>12/13</sub>-mCherry (Supplemental Fig. 2-4), FZD<sub>4</sub>-Cerulean also induced p115-RHOGEF-GFP membrane recruitment in combination with Gα<sub>12/13</sub>-mCherry (Fig. 8). Neither Gα<sub>12/13</sub>-mCherry nor FZD<sub>4</sub>-Cerulean alone was

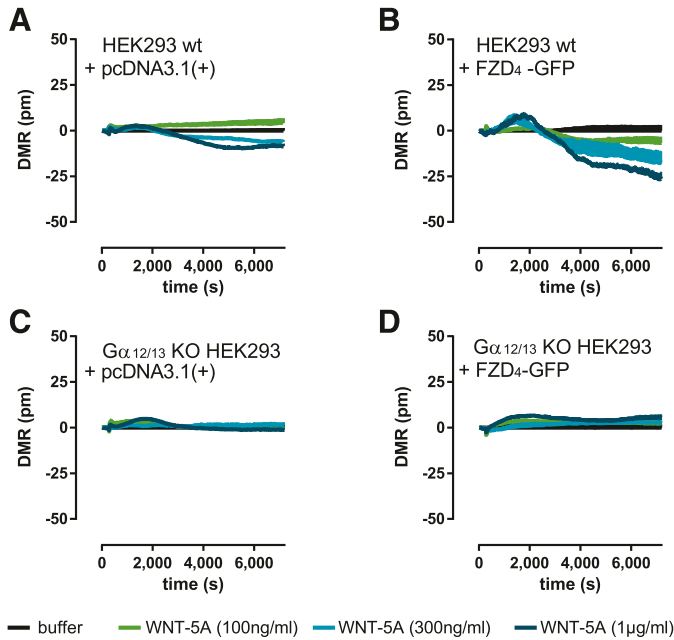


**Fig. 7.** WNT-induced dynamic mass redistribution depends on G $\alpha_{12/13}$  and FZD<sub>4</sub>-GFP. HEK293 wild-type (wt) cells and HEK293 cells lacking G $\alpha_{12/13}$  were stimulated with increasing amounts of WNT-5A (100, 300, and 1000 ng/ml). Changes in DMR were recorded over time. The apparent negative, WNT-5A-induced DMR responses in empty vector (A) or FZD<sub>4</sub>-GFP-transfected (B) HEK293 cells were not observed in the absence of G $\alpha_{12/13}$  proteins (C and D). Experiments were done after overnight treatment with the porcupine inhibitor C59 (5  $\mu$ M) at 37°C. Shown are representative traces ( $N = 3$ ), buffer-corrected and measured in triplicates + S.E.M. See Supplemental Fig. 5 for expression levels of FZD<sub>4</sub>-GFP and forskolin-induced DMR responses of wt and G $\alpha_{12/13}$ -knockout (KO) HEK293 cells.

sufficient to translocate p115-RHOGEF-GFP from a predominantly cytosolic expression pattern to a plasma membrane localization (Fig. 8; Supplemental Fig. 2). Substantial p115-RHOGEF-GFP membrane localization was only observed when FZD<sub>4</sub>-Cerulean was coexpressed with G $\alpha_{12/13}$ -mCherry, suggesting that receptor-induced activation of G $\alpha_{12/13}$  is required for this process.

To dissect the ligand dependence of the response from FZD<sub>4</sub> via G $\alpha_{12/13}$  to p115-RHOGEF-GFP recruitment, we disrupted endogenous secretion of WNTs by overnight treatment with the pharmacological porcupine inhibitor C59 (Proffitt et al., 2013). Porcupine was identified as a segment polarity gene giving rise to a multispan transmembrane protein catalyzing WNT acylation (Kadowaki et al., 1996). Pharmacological inhibition of porcupine is therefore an efficient way to decrease the amount of endogenously produced, functional WNTs to reduce autocrine stimulation (Dodge et al., 2012). This setup is analogous to the reduction of the LPA<sub>1</sub> receptor-induced and G $\alpha_{12/13}$ -mediated p115-RHOGEF-GFP recruitment by the LPA<sub>1</sub> receptor-selective antagonist/inverse agonist Ki16425 (Supplemental Fig. 4). In agreement with this, C59 treatment of cells transfected with FZD<sub>4</sub>-Cerulean, G $\alpha_{12/13}$ -mCherry, and p115-RHOGEF-GFP decreased the number of cells showing a membranous localization of p115-RHOGEF-GFP (Fig. 8), indicating that the endogenously secreted WNTs signal through FZD<sub>4</sub>-GFP and G $\alpha_{12/13}$ -mCherry to contribute to p115-RHOGEF-GFP recruitment.

G $\alpha_{12/13}$  need to be activated and GTP-bound to physically interact with p115-RHOGEF and simultaneously p115-

RHOGEF exerts GTPase activating protein or RGS activity on the heterotrimeric G protein to mediate inactivation as part of a negative feedback loop (Hart et al., 1998; Kozasa et al., 1998). To corroborate the FZD<sub>4</sub>-mediated activation of G $\alpha_{12/13}$ , we used the p115-RHOGEF-GFP recruitment as readout in cells cotransfected with the extended AU1-tagged RGS domain of p115-RHOGEF, the domain that promotes hydrolysis of GTP to GDP. Compared with cells transfected with FZD<sub>4</sub>-GFP, G $\alpha_{12/13}$ -mCherry, and p115-RHOGEF-GFP, where we observed  $23 \pm 2\%$  (G $\alpha_{12}$ )/ $30 \pm 3\%$  (G $\alpha_{13}$ ) (mean  $\pm$  S.E.M.) cells with membranous p115-RHOGEF-GFP, coexpression of the RGS domain reduced p115-RHOGEF-GFP membrane recruitment to  $13 \pm 2\%$  (G $\alpha_{12}$ )/ $13 \pm 3\%$  (G $\alpha_{13}$ ), corresponding to values in the absence of FZD<sub>4</sub>-GFP transfection [ $14 \pm 2\%$  (G $\alpha_{12}$ )/ $15 \pm 3\%$  (G $\alpha_{13}$ )] (Fig. 9).

## Discussion

In the present study, we used cellular imaging approaches to investigate the interaction of FZD<sub>4</sub> with heterotrimeric G proteins in unprecedented depth. Combining the dcFRAP technique with FRET, we were able to identify FZD<sub>4</sub> as a receptor assembled with G $\alpha_{12}$  and G $\alpha_{13}$  based on experiments in a mammalian cellular system. Cellular-imaging experiments were corroborated using innovative technology enabling DMR measurements in living cells to dissect the role of G $\alpha_{12/13}$  in WNT-induced cellular responses. In addition, we explored the roles of the scaffold protein DVL in FZD<sub>4</sub>-G protein assembly and the connection of FZD<sub>4</sub>, G $\alpha_{12/13}$ , and signaling to RHO via p115-RHOGEF.

Ever since their discovery in *Drosophila melanogaster*, FZDs have been postulated as being GPCRs due to structural and functional resemblance to more conventional class A, B, and C GPCRs (Vinson et al., 1989; Park et al., 1994; Schulte and Bryja, 2007). In support of what was previously surmised, a great amount of functional evidence has been gathered over the past two decades confirming that FZDs can signal as GPCRs (Slusarski et al., 1997; Liu et al., 1999, 2001; Ahumada et al., 2002; Sheldahl et al., 2003; Katanaev et al., 2005; Katanaev and Buestorf, 2009; Schulte, 2010; Kilander et al., 2011; Koval and Katanaev, 2011; Halleskog et al., 2012; Dijksterhuis et al., 2014).

In the case of FZD<sub>4</sub>, a receptor that has been attributed a central role in retinal vascularization and related diseases, such as familial exudative vitreoretinopathy (Robitaille et al., 2002), no evidence suggesting interaction with heterotrimeric G proteins has been reported so far. Based on our data using a live-cell imaging dcFRAP approach, which has been successfully used to study GPCR-G protein interactions in the past (Qin et al., 2008, 2011; Kilander et al., 2014b), we show that FZD<sub>4</sub> interacts with G $\alpha_{12/13}$  but not representatives of other G protein subfamilies. The observed selectivity of FZD<sub>4</sub> for one but not all groups of heterotrimeric G proteins underlines the specificity of the dcFRAP assay and supports the use of overexpressed proteins. Since we were able to detect the inactive-state assembly of FZD<sub>4</sub> and G $\alpha_{12/13}$  in living cells, we can conclude that this receptor complex is rather stable under the given circumstances. It should be noted, however, that dcFRAP analysis is a population-based assay without single-molecule sensitivity, and that it does not allow definite quantification of the affinity of the receptor to the heterotrimeric G protein. Further, our data do not allow a conclusion

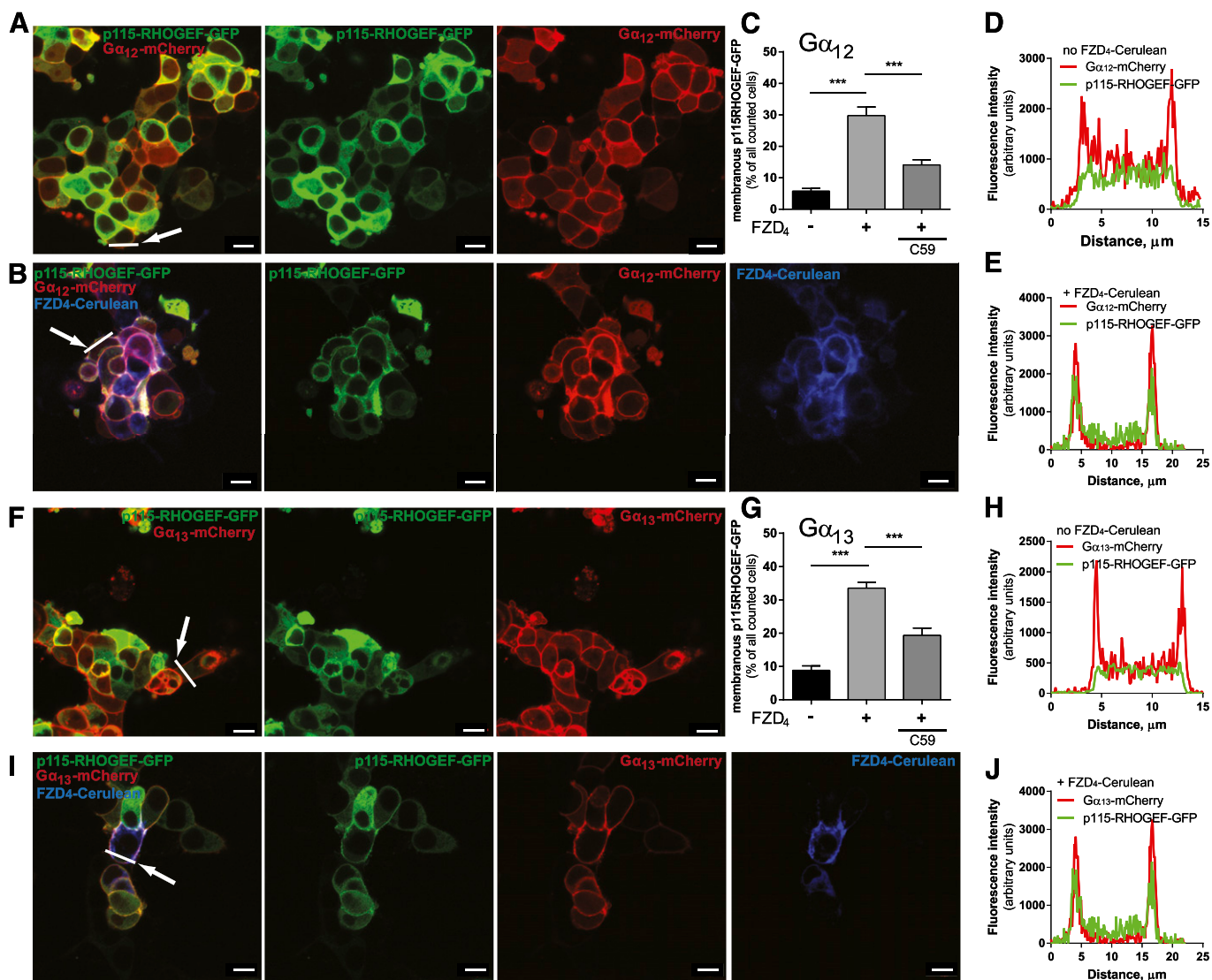


**Fig. 8.** FZD<sub>4</sub> induces p115-RHOGEF-GFP membrane recruitment in a  $G\alpha_{12/13}$ - and WNT-dependent manner. (A, B, F, and I) HEK293 cells were cotransfected with combinations of FZD<sub>4</sub>-Cerulean,  $G\alpha_{12}$ - or  $G\alpha_{13}$ -mCherry, and p115-RHOGEF-GFP and examined by live-cell confocal imaging. p115-RHOGEF-GFP showed an even cytosolic distribution when expressed alone or in combination with either  $G\alpha_{12}$ / $G\alpha_{13}$ -mCherry or FZD<sub>4</sub>-Cerulean (see Supplemental Fig. 2). The combination of FZD<sub>4</sub>-Cerulean and either  $G\alpha_{12}$ - or  $G\alpha_{13}$ -mCherry increased p115-RHOGEF-GFP plasma membrane localization. Quantification of the FZD<sub>4</sub>-Cerulean-dependent p115-RHOGEF-GFP recruitment was done by counting cells showing membranous versus cytosolic p115-RHOGEF-GFP distribution. Data from three independent experiments (>300 cells from several visual fields counted per condition for each individual experiment) are presented in the bar graphs (C and G). Data represent cells with a membranous p115-RHOGEF-GFP localization calculated as the percentage of total p115-RHOGEF-GFP-positive cells counted. In combination with the porcine inhibitor C59 (5  $\mu$ M; overnight treatment), FZD<sub>4</sub>-Cerulean-induced and  $G\alpha_{12}$ - or  $G\alpha_{13}$ -mCherry-mediated p115-RHOGEF-GFP recruitment was significantly reduced. Error bars provide the S.E.M. \*\*\* $P < 0.001$  ( $N = 3$ ). Cellular distribution profiles of p115-RHOGEF-GFP (green) and  $G\alpha_{12}$  or  $G\alpha_{13}$ -mCherry (red) fluorescence intensity along a line drawn over a single cell shown in (A, B, F, and I) (see arrow) in either the absence or presence FZD<sub>4</sub>-Cerulean are shown in (D, E, H, and J). Size bars = 10  $\mu$ m.

about the predominant mode of FZD<sub>4</sub>-G protein coupling in cells endogenously expressing the proteins, which could be cell-type and receptor expression level dependent. Thus, it remains to be resolved if FZD<sub>4</sub> at endogenous expression levels indeed forms an inactive-state complex with  $G\alpha_{12/13}$  or if the predominant mode of signaling is based on collision coupling.

To understand the structural basis of FZD-G protein selectivity, we performed C-terminal tail-swap experiments with FZD<sub>4</sub> and FZD<sub>6</sub>, of which the latter assembles with  $G\alpha_{i/q}$  (Kilander et al., 2014a,b). Whereas G protein selectivity of FZD<sub>6</sub> with the C terminus of FZD<sub>4</sub> was changed from

predominant  $G\alpha_i$  or  $G\alpha_q$  to  $G_{12/13}$ , FZD<sub>4</sub>  $G\alpha_{12/13}$  selectivity was not affected by exchanging the 41 aa C terminus to the 211 aa C terminus of FZD<sub>6</sub> (Fig. 6). Thus, it appears that  $G\alpha_{12/13}$  assembly can be achieved with structural determinants encoded by the FZD<sub>4</sub> and FZD<sub>6</sub> core, irrespective of the C-terminal tail. On the other hand, assembly with  $G\alpha_i$  or  $G\alpha_q$  is not determined by either the FZD<sub>6</sub> C terminus or the core alone, but it rather requires the combination of both in the intact FZD<sub>6</sub>. In this context, it should be noted that some structural features are common to both the FZD<sub>4</sub> and the FZD<sub>6</sub> C terminus, such as the conserved KTxxxW sequence and the potential ability to form a helix 8 (Schulte, 2010).



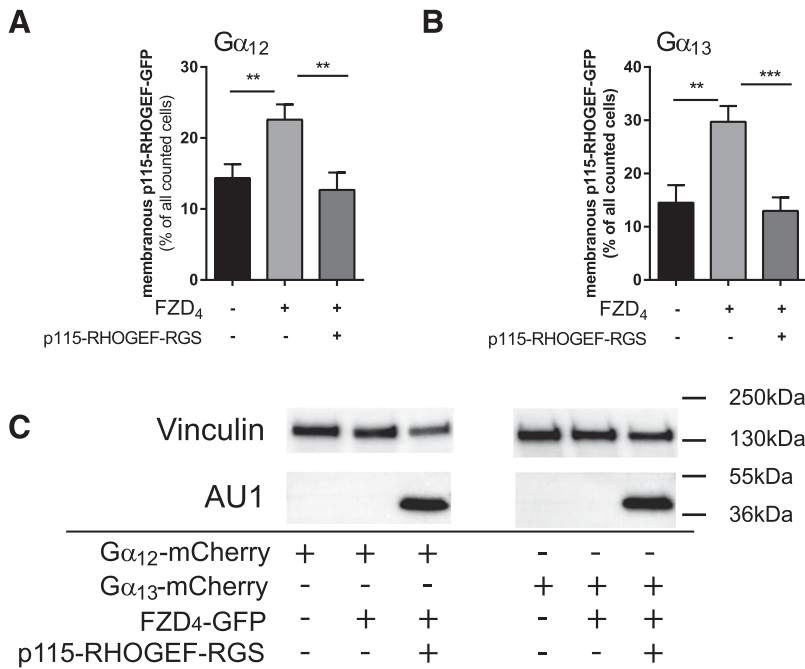


**Fig. 9.** FZD<sub>4</sub>-induced and G $\alpha_{12/13}$ -mediated p115-RHOGEF-GFP membrane recruitment depends on activation of the heterotrimeric G $\alpha_{12/13}$  proteins. HEK293 cells were transfected with FZD<sub>4</sub>-Cerulean, G $\alpha_{12}$ -mCherry (A) or G $\alpha_{13}$ -mCherry (B), and p115-RHOGEF-GFP either without or with the isolated AU1-tagged RGS domain of p115-RHOGEF-RGS. Cells presenting membranous p115-RHOGEF-GFP localization were counted, and data from four independent experiments were summarized in the bar graph. More than 50 cells were counted for each condition in each independent experiment. Values give the mean  $\pm$  S.E.M. (C) Cells used for quantification of p115-RHOGEF-GFP recruitment were lysed and immunoblotted for vinculin (loading control) and anti-AU1 to detect the tagged-RGS domain of p115-RHOGEF.

Furthermore, we found that this novel FZD<sub>4</sub>-G $\alpha_{12/13}$  liaison neither requires DVL for the formation of an inactive-state-assembled complex nor is sensitive to DVL overexpression. This stands in contrast to previous results, where we defined DVL as an essential component of the FZD<sub>6</sub>-G $\alpha_i$ /G $\alpha_q$  complex (Kilander et al., 2014b), arguing that the underlying mechanisms of FZDs interacting with heterotrimeric G proteins could be receptor isoform selective.

DMR analysis revealed G $\alpha_{12/13}$ -dependent WNT effects in both untransfected and FZD<sub>4</sub>-transfected HEK293 cells. It is well known that HEK293 cells endogenously express FZD<sub>4</sub>, among other FZDs (Atwood et al., 2011), suggesting that the WNT-G $\alpha_{12/13}$  responses measured in the receptor/G protein-overexpression paradigms can occur at endogenous receptor-G protein expression levels. Furthermore, the loss-of-function approach using HEK293 G $\alpha_{12/13}$  knockout cells underlines that the observed FZD<sub>4</sub>-G $\alpha_{12/13}$  liaison is not an artifact of receptor/G protein overexpression. On the other hand, these data open the possibility that other class FZD receptors expressed in HEK293 cells could also mediate signaling via G $\alpha_{12/13}$ .

Heterotrimeric G $\alpha_{12/13}$  proteins signal mainly to RHO GTPase-dependent pathways by interacting with several RHOGEFs, regulating, for example, changes in cell shape, migration, and adhesion (Worzfeld et al., 2008). In Figs. 8 and 9, we show that G $\alpha_{12/13}$ -induced p115-RHOGEF recruitment to the membrane is induced by FZD<sub>4</sub>. Since p115-RHOGEF interacts with the GTP-bound and active form of G $\alpha_{12/13}$  (Hart et al., 1998), which is dissociated from  $\beta\gamma$  subunits and the GPCR, this finding strongly argues not only that FZD<sub>4</sub> passively assembles with G $\alpha_{12/13}$ , but that FZD<sub>4</sub> is indeed capable of functionally coupling to G $\alpha_{12/13}$  acting as a GEF on these heterotrimeric G proteins. Given the lack of pharmacological tools for the selective stimulation of or interference with class Frizzled receptors, we instead used an alternative approach to pinpoint the ligand dependence of the FZD<sub>4</sub>/G $\alpha_{12/13}$ -mediated p115-RHOGEF-GFP recruitment. Pretreatment

with porcine inhibitors dramatically reduces autocrine WNT secretion (Proffitt et al., 2013), and the negative impact of C59 on p115-RHOGEF-GFP membrane localization argues that FZD<sub>4</sub>/G $\alpha_{12/13}$  signaling is WNT-dependent. In addition, the negative effect of the isolated p115-RHOGEF RGS domain acting as a G $\alpha_{12/13}$ -selective GTPase-activating protein (Hart et al., 1998; Kozasa et al., 1998) supports the functionality of the WNT-FZD<sub>4</sub>/G $\alpha_{12/13}$ -p115-RHOGEF signaling axis and its dependence on FZD<sub>4</sub>-mediated activation of G $\alpha_{12/13}$ .

In summary, our results provide the first evidence that FZD<sub>4</sub> and G $\alpha_{12/13}$  functionally interact, that WNTs can dissociate G $\alpha_{12/13}$  from the inactive-state complex, and that FZD<sub>4</sub>-G $\alpha_{12/13}$  mediate RHO signaling through membrane recruitment of p115-RHOGEF. Thus, FZD<sub>4</sub> should be seen as a G $\alpha_{12/13}$ -coupled GPCR, even though the circumstances that specify WNT signaling through the FZD<sub>4</sub>/G $\alpha_{12/13}$ /p115-RHOGEF signaling axis over the classic WNT/ $\beta$ -catenin pathway need to be defined in more detail.

#### Acknowledgments

The authors acknowledge Professor Lars Larsson (Department of Physiology and Pharmacology, Karolinska Institutet, Stockholm, Sweden) for providing generous access to the Zeiss LSM510 confocal microscope. The authors also thank Dr. Asuka Inoue (Graduate School of Pharmaceutical Sciences, Tohoku University) for providing parental and G $\alpha_{12/13}$  knockout HEK293 cells. The authors are grateful to Corning Inc. for support on the Epic DMR biosensor.

#### Authorship Contributions

*Participated in research design:* Arthofer, Hot, Grundmann, Kostenis, Gutkind, Schulte.

*Conducted experiments:* Arthofer, Hot, Petersen, Strakova, Jäger, Grundmann.

*Performed data analysis:* Arthofer, Hot, Petersen, Strakova, Jäger, Grundmann, Schulte.

*Wrote or contributed to the writing of the manuscript:* Arthofer, Hot, Petersen, Grundmann, Kostenis, Schulte.

## References

- Ahumada A, Slusarski DC, Liu X, Moon RT, Malbon CC, and Wang HY (2002) Signaling of rat Frizzled-2 through phosphodiesterase and cyclic GMP. *Science* **298**: 2006–2010.
- Angers S and Moon RT (2009) Proximal events in Wnt signal transduction. *Nat Rev Mol Cell Biol* **10**:468–477.
- Atwood BK, Lopez J, Wager-Miller J, Mackie K, and Straiker A (2011) Expression of G protein-coupled receptors and related proteins in HEK293, AtT20, BV2, and N18 cell lines as revealed by microarray analysis. *BMC Genomics* **12**:14.
- Ayoub MA, Al-Senaidy A, and Pin JP (2012) Receptor-G protein interaction studied by bioluminescence resonance energy transfer: lessons from protease-activated receptor 1. *Front Endocrinol (Lausanne)* **3**:82.
- Aznar N, Midde KK, Dunkel Y, Lopez-Sanchez I, Pavlova Y, Marivin A, Barbazán J, Murray F, Nitsche U, Janssen KP, et al. (2015) Daple is a novel non-receptor GEF required for trimeric G protein activation in Wnt signaling. *eLife* **4**:e07091.
- Bhattacharyya R and Wedegaertner PB (2000) Alpha 13 requires palmitoylation for plasma membrane localization, Rho-dependent signaling, and promotion of p115-RhoGEF membrane binding. *J Biol Chem* **275**:14992–14999.
- Bryja V, Schambony A, Cajánek L, Dominguez I, Arenas E, and Schulte G (2008) Beta-arrestin and casein kinase 1/2 define distinct branches of non-canonical WNT signalling pathways. *EMBO Rep* **9**:1244–1250.
- Clevers H and Nusse R (2012) Wnt/ $\beta$ -catenin signaling and disease. *Cell* **149**: 1192–1205.
- Digby GJ, Lober RM, Sethi PR, and Lambert NA (2006) Some G protein heterotrimers physically dissociate in living cells. *Proc Natl Acad Sci USA* **103**: 17789–17794.
- Dijksterhuis JP, Baljinnyam B, Stanger K, Sercan HO, Ji Y, Andres O, Rubin JS, Hannoush RN, and Schulte G (2015) Systematic mapping of WNT-FZD protein interactions reveals functional selectivity by distinct WNT-FZD pairs. *J Biol Chem* **290**:6789–6798.
- Dijksterhuis JP, Petersen J, and Schulte G (2014) WNT/Frizzled signalling: receptor-ligand selectivity with focus on FZD-G protein signalling and its physiological relevance: IUPHAR Review 3. *Br J Pharmacol* **171**:1195–1209.
- Dodge ME, Moon J, Tuladhara R, Lu J, Jacob LS, Zhang LS, Shi H, Wang X, Moro E, Mongera A, et al. (2012) Diverse chemical scaffolds support direct inhibition of the membrane-bound O-acyltransferase porcupine. *J Biol Chem* **287**:23246–23254.
- Dorsch S, Klotz KN, Engelhardt S, Lohse MJ, and Bünemann M (2009) Analysis of receptor oligomerization by FRAP microscopy. *Nat Methods* **6**:225–230.
- Galés C, Rebois RV, Hogue M, Trieu P, Breit A, Hébert TE, and Bouvier M (2005) Real-time monitoring of receptor and G-protein interactions in living cells. *Nat Methods* **2**:177–184.
- Galés C, Van Durm JJ, Schaak S, Pontier S, Percherancier Y, Audet M, Paris H, and Bouvier M (2006) Probing the activation-promoted structural rearrangements in preassembled receptor-G protein complexes. *Nat Struct Mol Biol* **13**:778–786.
- Grundmann M and Kostenis E (2015) Label-free biosensor assays in GPCR screening. *Methods Mol Biol* **1272**:199–213.
- Halleskog C, Dijksterhuis JP, Kilander MB, Becerril-Ortega J, Villaescusa JC, Lindgren E, Arenas E, and Schulte G (2012) Heterotrimeric G protein-dependent WNT-5A signaling to ERK1/2 mediates distinct aspects of microglia proinflammatory transformation. *J Neuroinflammation* **9**:111.
- Hart MJ, Jiang X, Kozasa T, Roscoe W, Singer WD, Gilman AG, Sternweis PC, and Bollag G (1998) Direct stimulation of the guanine nucleotide exchange activity of p115 RhoGEF by  $\alpha$ 13. *Science* **280**:2112–2114.
- Hart MJ, Sharma S, elMasry N, Qiu RG, McCabe P, Polakis P, and Bollag G (1996) Identification of a novel guanine nucleotide exchange factor for the Rho GTPase. *J Biol Chem* **271**:25452–25458.
- He X, Semenov M, Tamai K, and Zeng X (2004) LDL receptor-related proteins 5 and 6 in Wnt/ $\beta$ -catenin signaling: arrows point the way. *Development* **131**: 1663–1677.
- Hein P, Frank M, Hoffmann C, Lohse MJ, and Bünemann M (2005) Dynamics of receptor/G protein coupling in living cells. *EMBO J* **24**:4106–4114.
- Kadowaki T, Wilder E, Klingensmith J, Zachary K, and Perrimon N (1996) The segment polarity gene porcupine encodes a putative multitransmembrane protein involved in Wingless processing. *Genes Dev* **10**:3116–3128.
- Katanaev VL and Buestorf S (2009) Frizzled proteins are bona fide G protein-coupled receptors. *Nature Precedings* DOI: hdl:10101/npre.2009.2765.1.
- Katanaev VL, Ponzelli R, Sémériva M, and Tomlinson A (2005) Trimeric G protein-dependent frizzled signaling in Drosophila. *Cell* **120**:111–122.
- Kilander MB, Dahlström J, and Schulte G (2014a) Assessment of Frizzled 6 membrane mobility by FRAP supports G protein coupling and reveals WNT-Frizzled selectivity. *Cell Signal* **26**:1943–1949.
- Kilander MB, Petersen J, Andressen KW, Ganji RS, Levy FO, Schuster J, Dahl N, Bryja V, and Schulte G (2014b) Dishevelled regulates precoupling of heterotrimeric G proteins to Frizzled 6. *FASEB J* **28**:2293–2305.
- Kilander MB, Dijksterhuis JP, Ganji RS, Bryja V, and Schulte G (2011) WNT-5A stimulates the GDP/GTP exchange at pertussis toxin-sensitive heterotrimeric G proteins. *Cell Signal* **23**:550–554.
- Koval A and Katanaev VL (2011) Wnt3a stimulation elicits G-protein-coupled receptor properties of mammalian Frizzled proteins. *Biochem J* **433**:435–440.
- Kozasa T, Jiang X, Hart MJ, Sternweis PM, Singer WD, Gilman AG, Bollag G, and Sternweis PC (1998) p115 RhoGEF, a GTPase activating protein for  $\alpha$ 12 and  $\alpha$ 13. *Science* **280**:2109–2111.
- Lan TH, Kuravi S, and Lambert NA (2011) Internalization dissociates  $\beta$ 2-adrenergic receptors. *PLoS One* **6**:e17361.
- Liu T, DeCostanzo AJ, Liu X, Wang Hy, Hallagan S, Moon RT, and Malbon CC (2001) G protein signaling from activated rat frizzled-1 to the  $\beta$ -catenin-Lef-Tcf pathway. *Science* **292**:1718–1722.
- Liu X, Liu T, Slusarski DC, Yang-Snyder J, Malbon CC, Moon RT, and Wang H (1999) Activation of a frizzled-2/ $\beta$ -adrenergic receptor chimera promotes Wnt signaling and differentiation of mouse F9 teratocarcinoma cells via Galpho and Galphat. *Proc Natl Acad Sci USA* **96**:14383–14388.
- Macdonald BT, Semenov MV, and He X (2007) SnapShot: Wnt/ $\beta$ -catenin signaling. *Cell* **131**:1204.
- Meyer BH, Freuler F, Guerini D, and Siehler S (2008) Reversible translocation of p115-RhoGEF by G(12/13)-coupled receptors. *J Cell Biochem* **104**:1660–1670.
- Neubig RR (1994) Membrane organization in G-protein mechanisms. *FASEB J* **8**: 939–946.
- Nobles M, Benians A, and Tinker A (2005) Heterotrimeric G proteins precouple with G protein-coupled receptors in living cells. *Proc Natl Acad Sci USA* **102**: 18706–18711.
- Nusse R (2003) Wnts and Hedgehogs: lipid-modified proteins and similarities in signaling mechanisms at the cell surface. *Development* **130**:5297–5305.
- Offermanns S, Mancino V, Revel JP, and Simon MI (1997) Vascular system defects and impaired cell chemokinesis as a result of  $\alpha$ 13 deficiency. *Science* **275**: 533–536.
- Ohta H, Sato K, Murata N, Damirin A, Malchinkhuu E, Kon J, Kimura T, Tobo M, Yamazaki Y, Watanabe T, et al. (2003) Ki16425, a subtype-selective antagonist for EDG-family lysophosphatidic acid receptors. *Mol Pharmacol* **64**: 994–1005.
- Oldham WM and Hamm HE (2008) Heterotrimeric G protein activation by G-protein-coupled receptors. *Nat Rev Mol Cell Biol* **9**:60–71.
- Park WJ, Liu J, and Adler PN (1994) The frizzled gene of Drosophila encodes a membrane protein with an odd number of transmembrane domains. *Mech Dev* **45**: 127–137.
- Phair RD, Gorski SA, and Misteli T (2004) Measurement of dynamic protein binding to chromatin in vivo, using photobleaching microscopy. *Chromatin and Chromatin Remodeling Enzymes. Pt A* **375**:393–414.
- Proffitt KD, Madan B, Ke Z, Pendharkar V, Ding L, Lee MA, Hannoush RN, and Virshup DM (2013) Pharmacological inhibition of the Wnt acyltransferase PORCN prevents growth of WNT-driven mammary cancer. *Cancer Res* **73**: 502–507.
- Qin K, Dong C, Wu G, and Lambert NA (2011) Inactive-state preassembly of G(q)-coupled receptors and G(q) heterotrimers. *Nat Chem Biol* **7**:740–747.
- Qin K, Sethi PR, and Lambert NA (2008) Abundance and stability of complexes containing inactive G protein-coupled receptors and G proteins. *FASEB J* **22**: 2920–2927.
- Rasmussen SG, DeVree BT, Zou Y, Kruse AC, Chung KY, Kobilka TS, Thian FS, Chae PS, Pardon E, Calinski D, et al. (2011) Crystal structure of the  $\beta$ 2 adrenergic receptor-Gs protein complex. *Nature* **477**:549–555.
- Robitaille J, MacDonald ML, Kaykas A, Sheldahl LC, Zeisler J, Dubé FP, Zhang LH, Singaraja RR, Guernsey DL, Zheng B, et al. (2002) Mutant frizzled-4 disrupts retinal angiogenesis in familial exudative vitreoretinopathy. *Nat Genet* **32**: 326–330.
- Schröder R, Janssen N, Schmidt J, Kebig A, Merten N, Hennen S, Müller A, Blättermann S, Mohr-Andrä M, Zahn S, et al. (2010) Deconvolution of complex G protein-coupled receptor signaling in live cells using dynamic mass redistribution measurements. *Nat Biotechnol* **28**:943–949.
- Schröder R, Schmidt J, Blättermann S, Peters L, Janssen N, Grundmann M, Seemann W, Kaufel D, Merten N, Drewke C, et al. (2011) Applying label-free dynamic mass redistribution technology to frame signaling of G protein-coupled receptors noninvasively in living cells. *Nat Protoc* **6**:1748–1760.
- Schulte G (2010) International Union of Basic and Clinical Pharmacology. LXXX. The class Frizzled receptors. *Pharmacol Rev* **62**:632–667.
- Schulte G (2015) Frizzleds and WNT/ $\beta$ -catenin signaling—The black box of ligand-receptor selectivity, complex stoichiometry and activation kinetics. *Eur J Pharmacol* **763** (Pt B):191–195.
- Schulte G and Bryja V (2007) The Frizzled family of unconventional G-protein-coupled receptors. *Trends Pharmacol Sci* **28**:518–525.
- Semenov MV, Habas R, Macdonald BT, and He X (2007) SnapShot: Noncanonical Wnt Signaling Pathways. *Cell* **131**:1378.
- Shano S, Hatanaka K, Ninose S, Moriyama R, Tsujiuchi T, and Fukushima N (2008) A lysophosphatidic acid receptor lacking the PDZ-binding domain is constitutively active and stimulates cell proliferation. *Biochim Biophys Acta* **1783**:748–759.
- Shastry BS (2010) Genetic susceptibility to advanced retinopathy of prematurity (ROP). *J Biomed Sci* **17**:69.
- Sheldahl LC, Slusarski DC, Pandur P, Miller JR, Kühl M, and Moon RT (2003) Dishevelled activates Ca<sup>2+</sup> flux, PKC, and CamKII in vertebrate embryos. *J Cell Biol* **161**:769–777.
- Sivaraj KK, Takefuji M, Schmidt I, Adams RH, Offermanns S, and Wettschreck N (2013) G13 controls angiogenesis through regulation of VEGFR-2 expression. *Dev Cell* **25**:427–434.
- Slusarski DC, Corces VG, and Moon RT (1997) Interaction of Wnt and a Frizzled homologue triggers G-protein-linked phosphatidylinositol signalling. *Nature* **390**: 410–413.
- Tamai K, Semenov M, Kato Y, Spokony R, Liu C, Katsuyama Y, Hess F, Saint-Jeannet JP, and He X (2000) LDL-receptor-related proteins in Wnt signal transduction. *Nature* **407**:530–535.
- Toomes C, Downey LM, Bottomley HM, Mintz-Hittner HA, and Inglehearn CF (2005) Further evidence of genetic heterogeneity in familial exudative vitreoretinopathy: exclusion of EVR1, EVR3, and EVR4 in a large autosomal dominant pedigree. *Br J Ophthalmol* **89**:194–197.
- van Amerongen R and Nusse R (2009) Towards an integrated view of Wnt signaling in development. *Development* **136**:3205–3214.
- Vinson CR, Conover S, and Adler PN (1989) A Drosophila tissue polarity locus encodes a protein containing seven potential transmembrane domains. *Nature* **338**: 263–264.



- Warden SM, Andreoli CM, and Mukai S (2007) The Wnt signaling pathway in familial exudative vitreoretinopathy and Norrie disease. *Semin Ophthalmol* **22**:211–217.
- Wehrli M, Dougan ST, Caldwell K, O'Keefe L, Schwartz S, Vaizel-Ohayon D, Schejter E, Tomlinson A, and DiNardo S (2000) arrow encodes an LDL-receptor-related protein essential for Wingless signalling. *Nature* **407**:527–530.
- Worzfeld T, Wettschureck N, and Offermanns S (2008) G(12)/G(13)-mediated signalling in mammalian physiology and disease. *Trends Pharmacol Sci* **29**:582–589.
- Xu Q, Wang Y, Dabdoub A, Smallwood PM, Williams J, Woods C, Kelley MW, Jiang L, Tasman W, Zhang K, et al. (2004) Vascular development in the retina and inner ear: control by Norrin and Frizzled-4, a high-affinity ligand-receptor pair. *Cell* **116**:883–895.
- Yagi H, Tan W, Dillenburg-Pilla P, Armando S, Amornphimoltham P, Simaan M, Weigert R, Molinolo AA, Bouvier M, and Gutkind JS (2011) A synthetic biology approach reveals a CXCR4-G13-Rho signaling axis driving transendothelial migration of metastatic breast cancer cells. *Sci Signal* **4**:ra60.
- Ye X, Wang Y, Cahill H, Yu M, Badea TC, Smallwood PM, Peachey NS, and Nathans J (2009) Norrin, frizzled-4, and Lrp5 signaling in endothelial cells controls a genetic program for retinal vascularization. *Cell* **139**:285–298.
- Yu JZ and Rasenick MM (2002) Real-time visualization of a fluorescent G(alpha)(s): dissociation of the activated G protein from plasma membrane. *Mol Pharmacol* **61**: 352–359.

---

**Address correspondence to:** Dr. Gunnar Schulte, Karolinska Institutet, Department of Physiology and Pharmacology, Sec. Receptor Biology and Signaling, Nanna Svartz väg 2, S-171 77 Stockholm, Sweden. E-mail: gunnar.schulte@ki.se

---